Nitrate enhances anaerobic oxidation of methane in boreal lake sediments

Antti J Rissanen[1,*], Tom Jilbert[2], Asko Simojoki[3], Rahul Mangayil[1], Sanni L Aalto[4,5,a], Sari Peura[6], Helena Jäntti[4]

[1]Faculty of Engineering and Natural Sciences, Tampere University, Korkeakoulunkatu 6, FI-33720, Tampere, Finland

[2]Ecosystems and Environment Research Program, Faculty of Biological and Environmental Sciences, University of Helsinki, P.O. Box 65, FI-00014, Helsinki, Finland

[3]Department of Agricultural Sciences (Environmental Soil Science), Faculty of Agriculture and Forestry, University of Helsinki, P.O. Box 56, FI-00014, Helsinki, Finland

[4]Department of Environmental and Biological Sciences, University of Eastern Finland, Yliopistonranta 1 E, FI-70210, Kuopio, Finland

[5]Department of Biological and Environmental Sciences, University of Jyväskylä, Survontie 9 C, FI-40014, Jyväskylä, Finland

[6]Department of Forest Mycology and Plant Pathology, Science for Life Laboratory, Swedish University of Agricultural Sciences, Almas allé 5, SE-75651, Uppsala, Sweden

[a]Current address: Technical University of Denmark, DTU Aqua, Section for Aquaculture, The North Sea Research Centre, P.O. Box 101, DK-9850, Hirtshals, Denmark

*Corresponding author: Antti J Rissanen, Faculty of Engineering and Natural Sciences, Tampere University, Korkeakoulunkatu 6, FI-33720, Tampere, Finland. Tel: +358 40 1981145; Fax: +358 3 3641392; e-mail: antti.rissanen@tuni.fi

One sentence summary: Anaerobic oxidation of methane linked to nitrate reduction in boreal lake sediments

ABSTRACT

The importance of nitrate in promoting anaerobic oxidation of methane (AOM) in the sediments of boreal lakes is currently unknown. Here we investigated the extent to which sediment AOM is linked to nitrate reduction in a nitrate-rich, oligo-mesotrophic, boreal lake (Lake Pääjärvi, Finland). AOM potential of sediment slurries, collected from three profundal stations of the study lake, was measured at varying nitrate concentrations using ^{13}C-labelling. This was coupled with analysis of vertical profiles of the sediment and porewater geochemistry and the microbial communities (16S rRNA gene and shotgun metagenomic sequencing). Sediment AOM potential was enhanced by nitrate at a shallow station with high contents of labile phytoplankton-derived organic matter (Station 1), but not at the other two stations. AOM was also much higher at Station 1 (2.0-6.8 nmol C cm^{-3} d^{-1}) than at the other stations (0-0.3 nmol C cm^{-3} d^{-1}). Accordingly, methanotrophic archaea (*Candidatus* Methanoperedens sp.) and bacteria (*Methylococcales*) had the highest relative abundance at Station 1. Furthermore, geochemical profiles indicated that AOM was potentially coupled with reduction of nitrate, iron, or sulfate at all stations. We conclude that AOM linked to nitrate reduction takes place in boreal lake sediments. However, our data cannot resolve whether nitrate affects the process directly, via enhancing nitrate reduction-mediated AOM, or indirectly, via enhancing AOM mediated by reduction of other electron acceptors.

Keywords: anaerobic oxidation of methane, lake, methanotroph, sediment, shotgun metagenomics, 16S rRNA gene

INTRODUCTION

The concentration of atmospheric methane (CH_4), which is a critical greenhouse gas, has increased substantially since industrialization, with current total emissions 550 – 600 Teragrams/year (Saunois *et al.* 2020). Roughly 40 % of these emissions stem from natural sources (Saunois *et al.* 2020), being mostly produced by archaea in methanogenesis. Lakes are important natural emitters of CH_4 (Bastviken *et al.* 2011). The numerous lakes and ponds in the northern boreal zone with annual emissions of ~16.5 Tg (~7% of natural release) are especially significant contributors to the global CH_4 budget (Wik *et al.* 2016). Thus, knowledge about the factors affecting CH_4 emissions from northern lakes is essential for accurate estimates and modelling of global CH_4 budget.

Besides methanogenesis, microbial oxidation of CH_4 taking place in sediments and water columns is an important controller of the CH_4 emissions from lake ecosystems (Deutzmann *et al.* 2014). A recent study has reported that the anaerobic oxidation of methane (AOM) consumes large proportions (12 – 87 %) of gross CH_4 production in sediments of some boreal lakes (Martinez-Cruz *et al.* 2018). Nevertheless, contrasting observations (i.e. negligible role of AOM in reducing CH_4 emissions) from other boreal lakes have been also reported (Rissanen *et al.* 2017; Kallistova *et al.* 2018). This discrepancy can be due to varying availabilities of AOM-driving electron acceptors (EAs, i.e. NO_3^-, NO_2^-, Fe^{3+}, Mn^{4+}, SO_4^{2-} and organic EAs) between lakes. However, the identity of EAs driving AOM in lake sediments is understudied and such data is especially scarce from boreal lakes (Rissanen *et al.* 2017; Kallistova *et al.* 2018; Martinez-Cruz *et al.* 2018). In the few previous studies, additions of Fe^{3+}, Mn^{4+}, SO_4^{2-} or NO_3^- did not enhance AOM in sediments of boreal lakes (Rissanen *et al.* 2017; Kallistova *et al.* 2018). This was despite the fact that the sediments harbored typical freshwater AOM organisms, i.e.

archaea in genus *Ca*. Methanoperedens sp. (also known as ANME-2D archaea), that potentially use a wide variety of EAs (e.g. NO_3^-, Fe^{3+}, Mn^{4+} and SO_4^{2-}), and bacteria of genus *Ca*. Methylomirabilis sp. (within phylum *NC10*), that use NO_2^- (Ettwig *et al.* 2010; Haroon *et al.* 2013; Ettwig *et al.* 2016; Rissanen *et al.* 2017; Weber, Habicht and Thamdrup 2017). Previously, NO_3^-/NO_2^- was shown to drive AOM in sediments of a eutrophic NO_3^- - rich lake and a pond in temperate area (Deutzmann *et al.* 2014; Norði and Thamdrup 2014). Such data do not exist from NO_3^- - rich boreal lakes.

To shed light on the identity of EAs driving AOM in boreal lakes, we studied the effect of NO_3^- additions on AOM in sediments of a NO_3^- - rich boreal lake, Lake Pääjärvi (Southern Finland). The associated microbial communities were also studied using 16S rRNA gene sequencing and shotgun metagenomics. We hypothesized that due to the high availability of NO_3^-, AOM is linked to NO_3^- reduction, and, thus, NO_3^- addition enhances AOM in the sediments of the studied lake.

MATERIALS AND METHODS

Study lake

Lake Pääjärvi is a NO_3^- - rich, oligo-mesotrophic lake in southern Finland (61.04N, 25.08E; A = 13.4 km^2, max. depth = 87 m, mean residence time = 3.3 years). The water column circulates twice per year and is always well oxygenated (Salonen 1981). The large catchment area of Lake Pääjärvi (244 km^2) is dominated by forests and agriculture. Since the 1970s, the color and nutrient concentrations of the water have increased (Arvola *et al.* 1996).

Porewater and sediment sampling

Vertical profiles of porewater and sediment samples were collected from three stations in Lake Pääjärvi on 9th August 2017 using a hand-held HTH/Kajak corer with plexiglass tubes (Table 1). The stations followed a water depth gradient, Station 1 being shallowest and Station 3 deepest (Table 1). The core tubes were pre-drilled with two vertical series of 4 mm holes (each at 2 cm resolution), then taped, in preparation for porewater sampling with Rhizons™ (Rhizosphere research products, Wageningen, Netherlands). Rhizon sampling automatically filters the porewaters at 0.15 µm into attached 10 ml syringes under vacuum. One vertical series of samples was taken for analysis of dissolved CH_4 and dissolved inorganic carbon (DIC). The syringes were pre-filled with 1 ml of 0.1M HNO_3 to immediately convert all DIC to CO_2. A known volume of N_2 gas headspace was injected into the syringes after sampling, and the samples were shaken to equilibrate the dissolved gases with the headspace. The subsamples of the headspace were then extracted into 3 mL Exetainers™ (Labco Limited, Lampeter, UK) and stored at room temperature (RT) until analysis (for full details see Jilbert et al. 2020). The second vertical series was taken for S, Fe, and P [by inductively coupled plasma atomic emission spectroscopy (ICP-OES)], NO_3^-, and volatile fatty acids (VFA) analysis. NO_3^- and VFA subsamples were stored frozen at -20 °C until analysis. The subsamples for ICP-OES were acidified with 1 M HNO_3 and stored at RT. After porewater sampling, the sediment cores were sliced into plastic bags at a resolution of 1 cm (0–10 cm) or 2 cm (>10 cm). The subsamples of 400 – 500 µl wet sediment were collected from the 0–10 cm interval of each station and stored frozen at -20 °C for DNA-based molecular microbiological analyses. The remaining wet sediment samples were stored frozen at -20 °C under N_2 until further processing.

Porewater and sediment bulk geochemical analysis

According to our standard protocols, all the Rhizon samples were sequentially washed with 0.01 M HNO_3 and MilliQ water before field sampling. Later, it was noticed that the washing procedure caused background contamination in the porewater NO_3^- measurements. The magnitude and variability of this contamination was tested by sampling a solution of MilliQ water through the Rhizon samplers in plastic syringes and determining the NO_3^- concentration of the extracted sample. The same procedure was repeated using both factory-clean (9 replicates) and 0.01M HNO_3-washed Rhizons (10 replicates). The difference between the mean NO_3^- values, determined from the factory-clean and washed Rhizon samples (30.0 µmol L^{-1}), was subtracted from all the porewater NO_3^- data of this study. For objectivity, we report here the corrected values, as well as the error margins representing the full range of observed contamination (16.8 µmol L^{-1} – 73.9 µmol L^{-1}). The porewater nitrate concentrations were determined according to Miranda et al. (2001), while the samples from the HNO_3 – contamination test were analyzed by QuikChem®8000 flow injection analyzer (Lachat Instruments, Hach Co., Loveland, CO, USA) according to Wood et al. (1967).

The S, Fe and P concentrations in the porewater samples were determined by ICP-OES (Thermo iCAP 6000, Thermo Fisher Scientific, Waltham, MA, USA). In this system, S is expected to be dominated by sulfate (SO_4^{2-}), Fe by Fe^{2+}, and P by orthophosphate ($H_2PO_4^-$), although in each case, other forms are possible. The porewater CH_4 and DIC concentrations were determined by gas chromatography (GC) as described in Jilbert et al. (2020). Briefly, the sample vials (Exetainers) were pressurized with helium (He) to 2.0 bar before loading into the GC (Agilent technologies 7890B GC system, Agilent Technologies, Santa Clara, Ca, USA). CH_4 was determined by flame-ionization detector (FID) and CO_2 by thermal conductivity detector (TCD).

The instrument simultaneously measures N_2 and O_2 + Ar (in TCD), from which a 100% sum can be calculated for estimation of CH_4 and CO_2 concentrations in the original sample, in ppm by volume. For a full description of the calculations, see Jilbert et al. (2020).

Sediment samples were freeze-dried, ground in an agate mortar and weighed into tin cups for carbon (C) and nitrogen (N) content determinations. Inorganic forms of C and N are assumed negligible in this setting, hence no prior acidification was applied to the samples. C and N contents were determined using elemental analyzer (LECO TruSpec Micro, LECO Corp., St. Joseph, MI, USA).

Porewater VFAs were analyzed using high performance liquid chromatography (HPLC) equipped with Shodex SUGAR column (300 mm × 8 mm, Phenomenex, Torrance, CA, USA), autosampler (SIL-20AC HT, Shimadzu, Kioto, Japan), refractive index detector (RID-10A, Shimadzu), and 0.01 M H_2SO_4 as the mobile phase. The HPLC samples were prepared as described in Salmela et al. (2018). The identification and quantification of the liquid metabolites were conducted using external standards.

Incubations for the AOM measurements

The sediment for the incubation experiments was collected from the same three stations, one week after the collection of porewater and sediment samples (15th Aug 2017), using plexiglass tubes (diameter = 7 cm) connected to a gravity corer (Table 1). The initial porewater profile data were used to select the optimum depth horizons for sampling sediments for the incubations. At each station, a 3 cm thick sediment slice was cut immediately below the layer at which the porewater Fe concentrations started to increase, indicating the onset of anaerobic remineralization processes and therefore a suitable depth interval for the incubation experiments.

The upper limits to the incubation slices are as follows: -1 cm at Station 1 (thus, layer 1 – 4 cm from surface); -3 cm at Station 2 (layer 3 – 6 cm) and -3 cm at Station 3 (layer 3 – 6 cm).

The sediment from each station was mixed in 1:1 ratio with filtered (0.6 µm glass fiber filter) water collected 50 cm above the sediment. The sediment slurry was prepared in a 1 L bottle and purged with N_2 for 10 min. Thereafter, the bottle was quickly capped with a septum and the headspace was purged again with N_2 for 5 min. To ensure anoxic conditions prior to the experiments, the bottle containing the sediment slurry was placed on a shaker table overnight at 5°C and 120 rpm to facilitate the removal of any residual O_2. Thereafter, the set-up of incubations was conducted in a glove bag with N_2 atmosphere. The sediment slurry was transferred into 12 ml glass vials (Exetainers) (2 ml of slurry per vial, altogether 57 vials), and filled with filtered (0.6 µm), anoxic, N_2-purged bottom water. Thereafter, sterile, anoxic, N_2-purged stock solution of KNO_3 was added to the vials in concentrations of 0, 10, 50, 100, 200 and 500 µmol L^{-1}. There were three vials per each NO_3^- concentration at each station. Furthermore, one vial at each station represented a non-incubated control sample (without KNO_3) of the slurry at the beginning of the experiment. The vials were capped with septum, followed by the addition of 100 µl of gaseous ^{13}C-labeled CH_4 (^{13}C = 99.9%, Cambridge Isotope Laboratories Inc., Tewksbury, MA, USA) into two vials per each NO_3^- concentration at each station. One vial per each NO_3^- concentration at each station was not amended with ^{13}C-CH_4 and hence was included as a non-labeled control. The vials were taken out of the glove bag, shaken for 3 minutes to aid the dissolution of the added methane and incubated on a shaker (120 rpm) at 5 °C in the dark for 20 – 22 hours.

After incubations, 3 ml of slurry per sample were injected into pre-evacuated He-filled 12 ml vials (Exetainers) (over-pressure was released from the He-filled vials before sampling), which

contained 300 µL of H_3PO_4 (85%) to ensure the transformation of DIC into CO_2. The samples were then stored inverted at +4 °C until the analysis. For NO_3^- and NO_2^- analysis, 2 ml of the filtered (0.2 µm) slurry samples, before (non-incubated control samples of the slurry at the beginning, see above) and after the incubation (incubated ^{13}C-labeled samples), were stored at -20 °C. Analyses of NO_3^- and NO_2^- were done according to Miranda et al. (2001).

Stable isotopic and concentration analyses of DIC

Stable isotopic and concentration analyses of DIC were performed using an Isoprime100 isotope ratio mass spectrometer (IRMS) (Elementar UK Ltd., Cheadle, UK) coupled to an Isoprime TraceGas pre-concentration unit. The isotopic data was calculated as the fractional abundance of ^{13}C, i.e. ^{13}F, in DIC, using equation 1.

$$^{13}F = \frac{^{13}C}{(^{13}C + {}^{12}C)} \quad (1)$$

Calculations

A simple two-component mixing model was applied for a first-order quantification of the relative contributions of terrestrial plant-derived and autochtonous phytoplankton-derived organic matter to the total sedimentary organic matter (% of total organic C). The calculation uses the molar N:C ratio of organic matter, and end-member values, N/C_{EM}, based on the studies of Goñi et al. (2003) and Jilbert et al. (2018):

$$\%OC_{phyt} = \frac{\left(N/C_{sample} - N/C_{EM-terr}\right)}{\left(N/C_{EM-phyt} - N/C_{EM-terr}\right)} \times 100 \quad (2)$$

$$\%OC_{terr} = 100 - \%OC_{phyt} \quad (3)$$

where $N/C_{EM\text{-}terr} = 0.04$, and $N/C_{EM\text{-}phyt} = 0.13$. The calculation assumes that terrestrial plant matter and phytoplankton are the only sources of organic material present in the samples, the N/C values are spatially and temporally fixed at the end-member values, and the values do not alter significantly during sedimentation and burial of organic matter.

AOM rates were determined from the production rate of excess ^{13}C-labeled DIC,

$$\text{Excess } ^{13}\text{C-DIC} = (^{13}F_L - {}^{13}F_n) \times C_{conc} \quad (4)$$

where C_{conc} is the concentration of DIC, and $^{13}F_L$ is the fractional abundance of ^{13}C in ^{13}C-labeled samples, while $^{13}F_n$ denotes that in non-labeled samples (see equation 1). Assuming that the excess ^{13}C-DIC was zero at the beginning, we used a single time point measurement, i.e. excess ^{13}C-DIC after the incubations, to determine the AOM rate, expressed as rate per dry weight (DW) or per volume of sediment per hour (nmol C g^{-1}_{DW} h^{-1} or nmol C cm^{-3} h^{-1}). The added amount of CH_4 (i.e. 100 µl, see above) corresponds to a concentration of approximately 320 µmol L^{-1}, which is on average 9 – 17 times higher than the natural CH_4 concentration in the depth layers chosen for the incubations (see Results and Discussion). Furthermore, considering that the slurry preparations led to only 1 mL of the original sediment to be added to each vial (i.e. 2 mL of 1:1 water:sediment – slurry added to each vial, see above), the added ^{13}C-labeled CH_4 was estimated to account of almost all (> 99 %) of CH_4 in the incubation vial. Thus, the measured production rates of excess ^{13}C-DIC represent potential AOM rates. The CH_4 oxidation in this study was determined solely based on the transfer of ^{13}C from CH_4 to DIC, and hence, the proportion of CH_4-C bound to the biomass was not taken into account.

Production of NO_2^-, i.e. $NO_{2\,prod}^-$, was determined from the change in NO_2^- concentration during incubations, i.e. NO_2^- concentration at the beginning (i.e. non-incubated control samples of the slurry at the beginning, see above) was subtracted from the NO_2^- concentration after the incubations (incubated ^{13}C-labeled samples). Net conversion rate of NO_3^- to other products, i.e. N_{conv1}, was determined using equation 5, and assuming that NO_2^- was produced solely from NO_3^- reduction, net conversion rate of $NO_3^{-\cdot}$ to products other than NO_2^-, N_{conv2}, was determined using equation 6,

$$N_{conv1}=(Nn + Na) - Ne \quad (5)$$

$$N_{conv2}=(Nn + Na) - Ne - NO_{2\,prod}^- \quad (6)$$

where Nn and Ne are the concentrations of NO_3^- in the slurry in the beginning (non-incubated control samples of the slurry at the beginning, see above) and after the incubations (incubated ^{13}C-labeled samples), respectively, while Na is the added concentration of NO_3^-.

DNA extraction

DNA was extracted from the frozen sediment samples using DNeasy PowerSoil Kit (Qiagen, Hilden, Germany). DNA concentration was measured using a Qubit 2.0 Fluorometer and a dsDNA HS Assay Kit (Thermo Fisher Scientific, Waltham, MA, USA).

16S rRNA gene amplicon sequencing

PCR and 16S rRNA gene amplicon sequencing was performed by The Foundation for the Promotion of Health and Biomedical Research of Valencia Region (FISABIO, Valencia, Spain).

In the PCR reactions, the V4 region of the bacterial and archaeal 16S rRNA genes were simultaneously targeted using primer pair 515FB (5'-GTGYCAGCMGCCGCGGTAA-3´)/806FB (5'-GGACTACNVGGGTWTCTAAT-3´) (Apprill *et al.* 2015; Parada, Needham and Fuhrman 2016). PCR, library preparation and sequencing (Illumina MiSeq, Illumina, San Diego, CA, USA) was performed as previously described (Myllykangas *et al.* 2020), except that, in PCR reactions, approximately 15 ng of DNA were used.

Shotgun metagenomic sequencing

The shotgun metagenomic sequencing was performed by Novogene Co.,Ltd (Hong Kong). The libraries were prepared from ~100 ng of DNA per sample using the NEBNext® Ultra™ DNA Library Prep Kit for Illumina® (New England Biolabs, Ipswich, MA, USA) according to the manufacturer´s protocol. The sequencing was done on Illumina HiSeq X Ten System (Illumina) with paired-end mode and 150 bp read length producing from ~9 to ~12 Gb of raw data per sample.

Bioinformatic analyses of 16S rRNA gene data

The quality assessment of the raw sequence reads, merging of paired end reads, alignment, chimera removal, preclustering, taxonomic classification (and removal of chloroplast, mitochondria, and eukaryote sequences) and division of 16S rRNA gene sequences into operational taxonomic units (OTUs) at 97 % similarity level was conducted as previously described (Rissanen *et al.* 2020). Singleton OTUs (OTUs with only 1 sequence) were removed, and the data were then normalized by subsampling to the same size, 77340 sequences. One

sample, representing the layer 8-9 cm depth at Station 3, was discarded from the analyses since it had only ~10 000 sequences.

Bioinformatic analysis of shotgun metagenomic data

The raw sequences were analyzed using EBI Metagenomics pipeline (version 4.1) for trimming and taxonomic analysis of the reads containing 16S rRNA gene sequences against Silva 132 database (Mitchell *et al.* 2017). Furthermore, Kaiju web server (http://kaiju.binf.ku.dk/server) was used for taxonomic classification of the raw reads against National Center for Biotechnology Information´s (NCBI) nr – database (Menzel, Ng and Krogh 2016).

For metagenomic binning analysis, the raw data was trimmed using Trimmomatic (version 0.39) (Bolger, Lohse and Usadel 2014). The trimmed data was assembled using Megahit (version 1.2.8) (Li *et al.* 2015). The quality-controlled reads were mapped to the assembly using BBmap (version 38.73) (https://sourceforge.net/projects/bbmap/). The mapping results were used to bin the contigs using Metabat2 (Kang *et al.* 2015, 2019). The genes of the obtained metagenomic bins were predicted and annotated using Prokka (version 1.14.5) (Seemann 2014). The bins were also taxonomically annotated using CAT/BAT – tool and NCBI´s nr – database and taxonomy (von Meijenfeldt *et al.* 2019). Prokaryotic completeness and redundancy were computed using CheckM (version v1.1.2) (Parks *et al.* 2015). Taxonomic annotations were specifically screened for bins affiliated to known aerobic (gamma- and alphaproteobacterial MOBs) and anaerobic methanotrophs (ANME archaea and *Ca*. Methylomirabilis sp. bacteria). Furthermore, functional annotations were specifically screened for bins coding for particulate and soluble methane mono-oxygenases, key enzymes in aerobic methanotrophy and in *Ca*. Methylomirabilis sp. – mediated AOM, and for methyl coenzyme M reductase, the key enzyme in methanogenesis and in ANME archaea - mediated AOM.

Statistical analyses

The effect of varying NO_3^- concentration on AOM, NO_3^- consumption (N_{conv1} and N_{conv2}) and NO_2^- production at each station was studied using Spearman correlation analysis. In addition, for stations where NO_3^- and AOM correlated significantly, Michaelis-Menten kinetic - curve parameters (i.e. V_{max} = the maximum AOM rate achieved at saturating NO_3^- concentration; K_m = the NO_3^- concentration at which AOM rate is half of V_{max}) were estimated for AOM using non-linear regression analysis. The variation between stations in AOM, NO_3^- consumption and NO_2^- production was tested using randomized block analysis of variance (RB-ANOVA) with NO_3^- concentration level as the blocking factor. The average of two ^{13}C-labeled replicates per each NO_3^- concentration level was used as test values for AOM, N_{conv1}, N_{conv2} and NO_2^- production in the afore-mentioned correlation, non-linear regression and RB-ANOVA analyses.

In addition, the variation between stations in relative abundance of different methanotrophic, methanogenic and SO_4^{2-} reducing taxa at the depth layers representing the AOM incubation depths was analyzed using RB-ANOVA with depth layer (three 1 cm layers at each station) as the blocking factor. RB-ANOVA was followed by pair-wise post-hoc tests using the least significant difference (LSD) technique with Hochberg-Bonferroni-corrected α-values. Furthermore, the coherence in depth patterns between ANME archaea and SO_4^{2-} reducing bacteria was analyzed by Spearman correlation analysis. All the analyses were done using IBM SPSS Statistics 26 (IBM SPSS Statistics for Windows, Version 26.0, IBM Corp., Armonk, NY, USA).

Sequence database accession

The sequences of the 16S rRNA gene amplicon dataset are deposited in NCBI´s Sequence Read Archive (SRA) under the accession number PRJNA627335. The sequences of the shotgun metagenomic dataset are deposited in European Nucleotide Archive (ENA) under the accession number PRJEB29513.

RESULTS AND DISCUSSION

Sediment chemical characteristics and the structure of the methanogenic community

All the stations showed a broadly similar diagenetic zonation based on the porewater chemistry (Figs. 1 and 2). The vertical profiles of porewater concentrations of NO_3^-, S (assumed to be mostly SO_4^{2-}), Fe (assumed to be mostly Fe^{2+}, from reduction of solid-phase Fe oxides) and CH_4 suggest a transition zone, wherein the upwards-diffusing CH_4 is consumed by anaerobic respiration linked to reduction of NO_3^-, SO_4^{2-}, and Fe oxides. This zone was slightly closer to the sediment surface at Station 1 than at the other stations (Figs. 1 and 2). Station 1 also had higher overall concentrations of CH_4 and CO_2 than Station 2 and 3 (Fig. 2). Station 1 was also the only station at which lactate was observed in the porewaters (Fig. 2). In addition, while acetate and propionate were observed at all stations, they were at slightly higher levels at Station 1 than at the other two stations (Fig. 2). These results suggest that there was lower redox-potential and higher degree of fermentation at Station 1, leading to high rates of VFA production and methanogenesis. This may be due to higher availability of labile organic matter, being supported by our estimates on the contribution (%) of phytoplankton-derived organic carbon, which was slightly higher at Station 1 than at Station 2 and 3 (Fig. 2).

In accordance with the higher rates of methanogenesis at Station 1, the relative abundance of methanogens [shown as average % (min-max) of 16S rRNA gene amplicons] in the studied layer (topmost 10 cm) was generally higher there [0.5 % (0.01-1.1 %)] than at Station 2 [0.3 % (0.006-1.8 %)] and 3 [0.1 % (0.003-0.5 %)] (Fig. 3). The order *Methanomassiliicoccales*, whose cultivated members drive solely the hydrogenotrophic (i.e. H_2 oxidizing) methyl reducing methanogenic pathway, dominated the methanogen communities at each station (Borrel *et al.* 2013) (Fig. 3). Nevertheless, the hydrogenotrophic CO_2 reducing methanogens of the order *Methanomicrobiales* made also a significant proportion of methanogenic community at Station 1 but not at the other two stations (Nazaries *et al.* 2013) (Fig. 3). The dominance of *Methanomassiliicoccales* is surprising, because methanogenesis in freshwater sediments is typically dominated by the acetoclastic (i.e. acetate – utilizing) and hydrogenotrophic CO_2 reducing pathways (Conrad 1999). However, a recent metagenomic data suggested the presence of the acetoclastic pathway in genomes of uncultivated *Methanomassiliicoccales*, which could explain our findings (Speth and Orphan 2018). Unfortunately, we could not construct metagenome-assembled genomes (MAGs) of *Methanomassiliicoccales* or any other methanogens, probably because they had too low abundance to be caught by the metagenomic binning analysis (see Supplementary Results and Table S1). Hence, the potential functions of *Methanomassiliicoccales* in sediments of the study lake remain uncharacterized.

Potential AOM rates in the sediment

The effect of NO_3^- addition on potential AOM rates in sediment slurries consisting of layer 1 – 4 cm (from surface) at Station 1 and layer 3 – 6 cm at Station 2 and 3 was analyzed in anaerobic incubations using ^{13}C-labeled CH_4. The chosen layers exhibited active reduction of NO_3^-, SO_4^{2-} and Fe^{3+} and oxidation of CH_4, based on the vertical porewater profiles (Figs. 1-3).

The potential AOM rates were significantly higher at Station 1 (min-max: 0.5 – 1.8 nmol C g^{-1}_{DW} h^{-1}) than at Station 2 (0 – 0.07 nmol C g^{-1}_{DW} h^{-1}) and 3 (0 – 0.06 nmol C g^{-1}_{DW} h^{-1}) (RB-ANOVA, $F = 91$, $p < 0.001$), which did not differ from each other (Fig. 4a). As hypothesized, increasing levels of NO_3^- enhanced AOM. The potential AOM rates correlated positively with NO_3^- concentration at Station 1 ($\rho = 0.77$, $p < 0.05$), but not at Station 2 or 3 (Fig. 4a). However, the increase in the potential AOM rates was not linear at Station 1, roughly following Michaelis-Menten kinetics, which indicates NO_3^- - saturation of AOM within the range of the tested NO_3^- concentrations (added + natural, from 71 to 571 µmol L^{-1}) (Fig. 4a). The estimated K_m, 53 µmol L^{-1}, however, was outside of the range of the tested NO_3^- concentrations, which potentially decreases the reliability of the estimation. Comparing the Michaelis-Menten kinetic curve and K_m value with the estimated range of *in situ* NO_3^- in the incubation layers of Station 1, 0 – 22 µmol L^{-1}, we suggest that AOM is limited by NO_3^- availability in natural NO_3^- conditions (Figs. 3 & 4a).

NO_3^- was also consumed during the incubations at each station (Fig. 4b). However, N_{conv1} (NO_3^- conversion to other products) and N_{conv2} (NO_3^- conversion to other products than NO_2^-) did not differ between stations, whereas NO_2^- production was highest at Station 2, second highest at Station 3 and lowest at Station 1 (RB-ANOVA, $F = 49$, $p < 0.001$). Similar to its effects on AOM, NO_3^- additions enhanced NO_3^- consumption rates (Fig. 4b). N_{conv1} and N_{conv2} correlated with NO_3^- concentration at Station 3 (N_{conv1}: $\rho = 0.94$, $p < 0.01$; N_{conv2}: $\rho = 0.83$, $p < 0.05$). There was also a general tendency towards increasing NO_3^- consumption with increasing NO_3^- levels at Station 1 and 2, but these were statistically significant only when neglecting the deviant values at added NO_3^- concentration levels of 500 µmol L^{-1} at Station 1 and at 50 µmol L^{-1} and 100 µmol L^{-1} at Station 2 (N_{conv1}: $\rho = 1.0$, $p < 0.001$; N_{conv2}: $\rho = 1.0$, $p < 0.001$; at both stations) (Fig. 4b).

Hence, these results further indicate that NO_3^- was a limiting factor for NO_3^- consuming processes in the sediment in natural conditions. By contrast, NO_2^- production did not correlate with NO_3^- concentration (Fig. 4b).

Despite showing simultaneous NO_3^- - dependent increases in AOM and NO_3^- consumption, our data cannot confirm conclusively that NO_3^- was directly used as an EA in AOM. NO_3^- reduction can potentially affect CH_4 oxidation indirectly by promoting anaerobic oxidation of reduced sulfur and iron (to SO_4^{2-} and Fe^{3+}), thereby enhancing SO_4^{2-} - and Fe^{3+} dependent AOM (Klüber and Conrad 1998; Su *et al.* 2019). The possibility of Fe^{3+} and SO_4^{2-} - mediated AOM in Pääjärvi sediments is supported by the geochemical profiles (Figs. 1-3). Furthermore, reduction of NO_3^- and other N-oxides of the denitrification pathway (e.g. N_2O) could promote production/replenishment of organic EAs (e.g. humic substances), and hence indirectly support organic EA reduction - dependent AOM (Valenzuela *et al.* 2020).

The potential AOM rates in Pääjärvi (converted to volumetric rates, 0 – 6.8 nmol C cm^{-3} d^{-1}) are within the lower end of AOM rates reported from lake sediments in general (0 – 180 nmol C cm^{-3} d^{-1}) and from boreal lakes in particular (0 – 16.3 nmol C cm^{-3} d^{-1}) (Rissanen *et al.* 2017; Martinez-Cruz *et al.* 2018). However, the AOM rates at Station 1 (2.0 – 6.8 nmol C cm^{-3} d^{-1}) correspond well with the median AOM (3.5 nmol C cm^{-3} d^{-1}) of the multiple lake studies reviewed by Martinez-Cruz et al. (2018). The results are also in agreement with the NO_3^- - amended AOM rates from profundal zone of the eutrophic, NO_3^- - rich lake (L. Constance) (1.8 – 3.6 nmol C cm^{-3} d^{-1}) (Deutzmann and Schink 2011). In addition, the low rates at Station 2 (0 – 0.3 nmol C cm^{-3} d^{-1}) and 3 (0 – 0.2 nmol C cm^{-3} d^{-1}), where NO_3^- additions did not enhance AOM, are within the same range with the rates measured previously from two boreal lakes (0 - 0.3 nmol C cm^{-3} d^{-1}) where AOM was insignificant and similarly not enhanced by inorganic EAs

(Rissanen *et al.* 2017). For V_{max}, no comparison to previous studies can be made, as to our knowledge, V_{max} values have been previously estimated only for aerobic CH_4 oxidation but not for AOM taking place in lake sediments (Lidstrom and Somers 1984; Auman *et al.* 2000; Deutzmann, Wörner and Schink 2011). We are also not aware of any previous study estimating K_m for NO_3^--dependent AOM in lake sediments. However, the estimated K_m (i.e. 53 µmol L^{-1} NO_3^--N) for AOM in sediment slurries from Station 1 of the study lake is within the lower end of the range previously estimated for denitrification (measured using acetylene inhibition technique) in lake sediment slurries (3 – 1102 µmol L^{-1}) and significantly lower than the average (286 µmol L^{-1}) and the median K_m (219 µmol L^{-1}) calculated from the same data (including 20 lakes from Colorado and 1 lake from Florida) (Messer and Brezonik 1984; McCrackin and Elser 2012). The lower K_m for AOM than for denitrification actually suggests that AOM organisms have higher affinity for NO_3^- than denitrifiers, and hence would be more competitive for NO_3^- under natural conditions. However, this hypothesis needs confirmation in further studies estimating K_m of both AOM and denitrification in the same lake.

Methanotrophic community in the sediments

Aerobic MOBs, in order *Methylococcales* and family *Methylacidiphilaceae*, as well as anaerobic methanotrophs, in genera *Ca*. Methanoperedens sp. (also known as ANME 2D archaea), and *Ca*. Methylomirabilis sp. (within bacterial phylum *NC10*), were present in the studied sediments, agreeing with the previous study on boreal lake sediments (Rissanen *et al.* 2017) (Fig. 3). Alphaproteobacterial MOBs were rare and actually not even detected in the analysis of 16S rRNA gene amplicons.

Methanotroph communities in the depth layers representing the layers chosen for AOM incubation were compared between stations. *Ca*. Methanoperedens sp., *Methylococcales* and

total MOBs (consisting mostly of *Methylococcales*) had higher relative abundances at Station 1 than at other stations. However, with regards to the 16S rRNA gene reads in the shotgun metagenomic dataset, the difference for *Methylococcales* and total MOBs was not statistically significant (Fig. 5). The higher relative abundance of *Ca*. Methanoperedens at Station 1 than at other stations, validates the higher AOM rates obtained from Station 1. In addition, in NO_3^- rich systems such as the study lake, *Ca*. Methanoperedens sp. can directly couple AOM with reduction of NO_3^- (to NO_2^- or to NH_4^+) (Haroon *et al.* 2013; Welte *et al.* 2016; Nie *et al.* 2020), further supporting our findings on the positive effect of NO_3^- supplementation on AOM. Although *Methylococcales* are not considered to be anaerobic methanotrophs, they may include species that can couple CH_4 oxidation with NO_3^-/NO_2^- reduction in hypoxic and anoxic conditions (Kits, Klotz and Stein 2015; Martinez-Cruz *et al.* 2017; Oswald *et al.* 2017; Rissanen *et al.* 2018). Thus, the higher relative abundance of *Methylococcales* at Station 1 could further support the results on NO_3^- reduction-dependent CH_4 oxidation. As above for methanogens, we could not construct MAGs of *Methylococcales* or any other methanotrophic taxa, probably due to their too low abundance (see Supplementary Results and Table S1). However, according to our previous MAG studies, the *Methylococcales* genera that were dominant in the study lake, i.e. *Methylobacter* and *Crenothrix* (60 – 89 % of the 16S rRNA gene amplicons affiliated to *Methylococcales* in the study lake) (Fig. S1), include members that harbored genetic potential for denitrification in the hypoxic and anoxic water columns of closely located Lake Alinen-Mustajärvi (within 20 km from the study lake) and Lake Lovojärvi (within 4 km) (Rissanen *et al.* 2018, 2020). In addition, *Methylobacter* in boreal lake sediments have genetic potential for denitrification, as indicated by our functional annotation analysis (Prokka, version 1.14.5, Seemann 2014) finding genes coding for dissimilatory nitrate and nitrite reduction in two MAGs

representing genus *Methylobacter* in sediments of Lake Alinen Mustajärvi (NCBI accession no. GCA_903932065.1 and GCA_903870475.1; MAGs constructed/published by Buck *et al*. 2020).

Besides NO_3^-, *Ca*. Methanoperedens sp. archaea have been also suggested to use SO_4^{2-}, Fe^{3+} and organic compounds as EAs in AOM (Knittel and Boetius 2009; Ettwig *et al.* 2016; Timmers *et al.* 2017; Weber, Habicht and Thamdrup 2017; Bai *et al.* 2019; Su *et al.* 2019). Furthermore, recent evidence suggests that some members of *Methylococcales* transfer electrons from CH_4 to Fe^{3+} minerals and organic EAs while oxidizing CH_4 in hypoxic and anoxic conditions (Oswald *et al.* 2016; Zheng *et al.* 2020). Accordingly, genetic potential for extracellular electron transfer to metal minerals and organic EAs has been found in MAGs of *Methylococcales* in lake water columns (He *et al.* 2019; Rissanen *et al.* 2020). Furthermore, our functional annotation analysis (using FeGenie, Garber *et al*. 2020) of the aforementioned *Methylobacter* - MAGs from the sediments of Lake Alinen Mustajärvi found genetic potential for extracellular electron transfer in one of them (GCA_903870475.1). Altogether, these findings support the possibility that the observed NO_3^- mediated increase in CH_4 oxidation was indirect, via enhancement of SO_4^{2-} , Fe^{3+} and organic EA reduction-dependent AOM. ANME archaea drive SO_4^{2-} - dependent AOM usually in syntrophic relationship with SO_4^{2-} reducing bacterial partners (Knittel and Boetius 2009). The relative abundance of SO_4^{2-} reducing bacteria in the depth layers representing the AOM incubation layers did not vary between the stations (Fig. S2a). However, the vertical depth patterns of *Ca*. Methanoperedens and total SO_4^{2-} reducers ($\rho = 0.81$, $p < 0.01$) and the dominant SO_4^{2-} reducing taxa, i.e. *Desulfarculaceae* ($\rho = 0.67$, $p < 0.05$), *Desulfobacterales* ($\rho = 0.64$, $p < 0.05$) and *Desulfobacca* ($\rho = 0.71$, $p < 0.05$,) were coherent at Station 1 (Fig. S2b), where also the highest AOM rates and NO_3^- - enhancement of AOM were observed. In contrast, such coherent patterns were not observed for Station 2 and 3. Nevertheless, these results further hint

that SO_4^{2-} - mediated AOM can take place in sediments of the study lake and is potentially enhanced indirectly by NO_3^-. Recent results also suggest that besides ANME archaea, methanogens may drive AOM coupled with electron transfer to solid EAs, e.g. Fe^{3+} minerals (Bar-Or *et al.* 2017; Yu *et al.* 2021). However, none of the methanogenic taxa in the AOM incubation layers had a significantly higher relative abundance at Station 1 than at other stations (Fig. S3). Thus, variations in the methanogenic community did not explain the differences in the potential AOM rates between stations.

The putative NO_2^- reducing AOM-driving bacteria in the genus *Ca*. Methylomirabilis had a higher relative abundance than *Ca*. Methanoperedens archaea at each station (Figs. 3 and 5). Furthermore, their relative abundance was much higher upper in the sediment profile than within the incubation layers at Station 2 and 3 (Fig. 3). These results suggest that NO_2^-, produced in NH_4^+ oxidation and NO_3^- reduction near the oxic-anoxic interface in top-most layers of the sediments, might be an important EA for AOM in the study lake. Thus, despite *Ca*. Methylomirabilis did not vary in their relative abundance between stations at the depth layers representing the layers chosen for AOM incubations (Fig. 5), they potentially contributed to the AOM by coupling it to the reduction of NO_2^- in the study lake (Deutzmann *et al.* 2014; Welte *et al.* 2016).

CONCLUSION

Overall, our study is the first to show that AOM linked to NO_3^- reduction takes place in sediments of lakes of the boreal area. The results also strongly suggest that the process is mediated by *Ca*. Methanoperedens sp. archaea, with potential contribution from bacteria

belonging to *Methylococcales* and *Ca*. Methylomirabilis sp. Further studies could focus on elucidating whether the effect of NO_3^- on AOM was direct, via enhancement of NO_3^- reduction - mediated AOM, or indirect, via enhancement of AOM mediated by reduction of SO_4^{2-}, Fe^{3+} and organic EAs.

FUNDING

This study was supported by Academy of Finland (Grant No. 286642 for AJR, 323214 for RM, 307331 for HJ, and 310302 for SLA), joint funding by Olvi Foundation, Jenny and Antti Wihuri Foundation, and Saastamoinen Foundation (for HJ) and Kone Foundation (Grant No. 201803224 for AJR), and a Tenure Track starting package from University of Helsinki (TJ).

ACKNOWLEDGEMENTS

We thank M. McCrackin for providing K_m values of denitrification from her study lakes. We also thank staff at the Lammi Biological Station for their support in field and laboratory work.

Conflict of interest. None declared.

REFERENCES

Apprill A, McNally S, Parsons R *et al*. Minor revision to V4 region SSU rRNA 806R gene primer greatly increases detection of SAR11 bacterioplankton. *Aquat Microb Ecol* 2015;**75**:129–37.

Arvola L, Kankaala P, Tulonen T *et al*. Effects of phosphorus and allochthonous humic matter enrichment

on metabolic processes and community structure of plankton in a boreal lake (Lake Pääjärvi). *Can J Fish Aquat Sci* 1996;**53**:1646–62.

Auman AJ, Stolyar S, Costello AM *et al.* Molecular Characterization of Methanotrophic Isolates from Freshwater Lake Sediment. *Appl Environ Microbiol* 2000;**66**:5259 – 5266.

Bai Y-N, Wang X-N, Wu J *et al.* Humic substances as electron acceptors for anaerobic oxidation of methane driven by ANME-2d. *Water Res* 2019;**164**:114935.

Bar-Or I, Elvert M, Eckert W *et al.* Iron-Coupled Anaerobic Oxidation of Methane Performed by a Mixed Bacterial-Archaeal Community Based on Poorly Reactive Minerals. *Environ Sci Technol* 2017;**51**:12293–301.

Bastviken D, Tranvik LJ, Downing JA *et al.* Freshwater methane emissions offset the continental carbon sink. *Science* 2011;**331**:50.

Bolger AM, Lohse M, Usadel B. Trimmomatic: a flexible trimmer for Illumina sequence data. *Bioinformatics* 2014;**30**:2114–20.

Borrel G, O'Toole PW, Harris HM *et al.* Phylogenomic data support a seventh order of methylotrophic methanogens and provide insights into the evolution of methanogenesis. *Genome Biol Evol* 2013;**5**:1769–80.

Buck M, Garcia SL, Fernandez Vidal L et al. Comprehensive dataset of shotgun metagenomes from stratified freshwater lakes and ponds. bioRxiv 2020, DOI: https://doi.org/10.1101/2020.11.12.379446

Conrad R. Contribution of hydrogen to methane production and control of hydrogen concentrations in methanogenic soils and sediments. *FEMS Microbiol Ecol* 1999;**28**:193–202.

Deutzmann JS, Schink B. Anaerobic oxidation of methane in sediments of Lake Constance, an oligotrophic freshwater lake. *Appl Environ Microbiol* 2011;**77**:4429–36.

Deutzmann JS, Stief P, Brandes J *et al.* Anaerobic methane oxidation coupled to denitrification is the dominant methane sink in a deep lake. *Proc Natl Acad Sci U S A* 2014;**111**:18273–8.

Deutzmann JS, Wörner S, Schink B. Activity and diversity of methanotrophic bacteria at methane seeps in eastern Lake Constance sediments. *Appl Environ Microbiol* 2011;**77**:2573–81.

Ettwig KF, Butler MK, Le Paslier D *et al.* Nitrite-driven anaerobic methane oxidation by oxygenic bacteria. *Nature* 2010;**464**:543–8.

Ettwig KF, Zhu B, Speth D *et al.* Archaea catalyze iron-dependent anaerobic oxidation of methane. *Proc Natl Acad Sci* 2016;**113**:12792–6.

Garber AI, Nealson KH, Okamoto A et al. FeGenie: A comprehensive tool for the identification of iron genes and iron gene neighborhoods in genome and metagenome assemblies. *Front Microbiol* 2020;**11**:37.

Goñi MA, Teixeira MJ, Perkey DW. Sources and distribution of organic matter in a river-dominated estuary (Winyah Bay, SC, USA). *Estuar Coast Shelf Sci* 2003;**57**:1023–48.

Haroon MF, Hu S, Shi Y *et al.* Anaerobic oxidation of methane coupled to nitrate reduction in a novel archaeal lineage. *Nature* 2013;**500**:567–70.

He S, Lau MP, Linz AM *et al.* Extracellular Electron Transfer May Be an Overlooked Contribution to Pelagic Respiration in Humic-Rich Freshwater Lakes. *mSphere* 2019;**4**:e00436-18.

Jilbert T, Asmala E, Schröder C *et al.* Impacts of flocculation on the distribution and diagenesis of iron in boreal estuarine sediments. *Biogeosciences* 2018;**15**:1243–71.

Jilbert T, Jokinen S, Saarinen T *et al.* Impacts of a deep reactive layer on sedimentary phosphorus dynamics in a boreal lake recovering from eutrophication. *Hydrobiologia* 2020;**847**:4401–23.

Kallistova A, Kadnikov V, Rusanov I *et al.* Microbial communities involved in aerobic and anaerobic methane cycling in a meromictic ferruginous subarctic lake. *Aquat Microb Ecol* 2018;**82**:1–18.

Kang D., Froula J, Egan R *et al.* MetaBAT, an efficient tool for accurately reconstructing single genomes from complex microbial communities. *PeerJ* 2015;**3**:e1165.

Kang D., Li F, Kirton E *et al.* MetaBAT 2: an adaptive binning algorithm for robust and efficient genome reconstruction from metagenome assemblies. *PeerJ* 2019;**7**:e7359.

Kits KD, Klotz MG, Stein LY. Methane oxidation coupled to nitrate reduction under hypoxia by the Gammaproteobacterium Methylomonas denitrificans, sp. nov. type strain FJG1. *Environ Microbiol* 2015;**17**:3219–32.

Klüber HD, Conrad R. Effects of nitrate, nitrite, NO and N2O on methanogenesis and other redox processes in anoxic rice field soil. *FEMS Microbiol Ecol* 1998;**25**:301–18.

Knittel K, Boetius A. Anaerobic oxidation of methane: progress with an unknown process. *Annu Rev Microbiol* 2009;**63**:311–34.

Li D, Liu C-M, Luo R *et al.* MEGAHIT: an ultra-fast single-node solution for large and complex metagenomics assembly via succinct de Bruijn graph. *Bioinformatics* 2015;**31**:1674–6.

Lidstrom ME, Somers L. Seasonal Study of Methane Oxidation in Lake Washington. *Appl Environ Microbiol* 1984;**47**:1255 – 1260.

Martinez-Cruz K, Leewis M-C, Herriott IC *et al.* Anaerobic oxidation of methane by aerobic methanotrophs in sub-Arctic lake sediments. *Sci Total Environ* 2017;**607**:23–31.

Martinez-Cruz K, Sepulveda-Jauregui A, Casper P *et al.* Ubiquitous and significant anaerobic oxidation of methane in freshwater lake sediments. *Water Res* 2018;**144**:332–40.

McCrackin ML, Elser JJ. Denitrification kinetics and denitrifier abundances in sediments of lakes receiving atmospheric nitrogen deposition (Colorado, USA). *Biogeochemistry* 2012;**108**:39–54.

von Meijenfeldt FAB, Arkhipova K, Cambuy DD *et al.* Robust taxonomic classification of uncharted microbial sequences and bins with CAT and BAT. *Genome Biol* 2019;**20**:217.

Menzel P, Ng KL, Krogh A. Fast and sensitive taxonomic classification for metagenomics with Kaiju. *Nat Commun* 2016;**7**:11257.

Messer JJ, Brezonik PL. Laboratory evaluation of kinetic parameters for lake sediment denitrification models. *Ecol Modell* 1984;**21**:277–86.

Miranda KM, Espey MG, Wink DA. A Rapid, Simple Spectrophotometric Method for Simultaneous Detection of Nitrate and Nitrite. *Nitric Oxide* 2001;**5**:62–71.

Mitchell AL, Scheremetjew M, Denise H *et al.* EBI Metagenomics in 2017: enriching the analysis of microbial communities, from sequence reads to assemblies. *Nucleic Acids Res* 2017;**46**:D726–35.

Myllykangas J-P, Rissanen AJ, Hietanen S *et al.* Influence of electron acceptor availability and microbial community structure on sedimentary methane oxidation in a boreal estuary. *Biogeochemistry*

2020;**148**:291–309.

Nazaries L, Murrell JC, Millard P *et al.* Methane, microbes and models: fundamental understanding of the soil methane cycle for future predictions. *Environ Microbiol* 2013;**15**:2395–417.

Nie W-B, Ding J, Xie G-J *et al.* Anaerobic Oxidation of Methane Coupled with Dissimilatory Nitrate Reduction to Ammonium Fuels Anaerobic Ammonium Oxidation. *Environ Sci Technol* 2020, DOI: 10.1021/acs.est.0c02664.

Norði K á., Thamdrup B. Nitrate-dependent anaerobic methane oxidation in a freshwater sediment. *Geochim Cosmochim Acta* 2014;**132**:141–50.

Oswald K, Graf JS, Littmann S *et al.* Crenothrix are major methane consumers in stratified lakes. *Isme J* 2017;**11**:2124.

Oswald K, Milucka J, Brand A *et al.* Aerobic gammaproteobacterial methanotrophs mitigate methane emissions from oxic and anoxic lake waters. *Limnol Oceanogr* 2016;**61**:S101–18.

Parada AE, Needham DM, Fuhrman JA. Every base matters: assessing small subunit rRNA primers for marine microbiomes with mock communities, time series and global field samples. *Environ Microbiol* 2016;**18**:1403–14.

Parks DH, Imelfort M, Skennerton CT *et al.* CheckM: assessing the quality of microbial genomes recovered from isolates, single cells, and metagenomes. *Genome Res* 2015;**25**:1043–55.

Rissanen A, Saarenheimo J, Tiirola M *et al.* Gammaproteobacterial methanotrophs dominate methanotrophy in aerobic and anaerobic layers of boreal lake waters. *Aquat Microb Ecol* 2018;**81**:257–76.

Rissanen AJ, Karvinen A, Nykänen H *et al.* Effects of alternative electron acceptors on the activity and community structure of methane-producing and consuming microbes in the sediments of two shallow boreal lakes. *FEMS Microbiol Ecol* 2017;**93**:fix078.

Rissanen AJ, Saarela T, Jäntti H *et al.* Vertical stratification patterns of methanotrophs and their genetic controllers in water columns of oxygen-stratified boreal lakes. *FEMS Microbiol Ecol* 2020, DOI: 10.1093/femsec/fiaa252.

Salmela M, Lehtinen T, Efimova E *et al.* Metabolic pairing of aerobic and anaerobic production in a one-pot batch cultivation. *Biotechnol Biofuels* 2018;**11**, DOI: 10.1186/s13068-018-1186-9.

Salonen K. The ecosystem of the oligotrophic Lake Pääjärvi 2. Bacterioplankton. *SIL Proceedings, 1922-2010* 1981;**21**:448–53.

Saunois M, Stavert AR, Poulter B *et al.* The Global Methane Budget 2000–2017. *Earth Syst Sci Data* 2020;**12**:1561–623.

Seemann T. Prokka: rapid prokaryotic genome annotation. *Bioinformatics* 2014;**30**:2068–9.

Speth D, Orphan V. Metabolic marker gene mining provides insight in global mcrA diversity and, coupled with targeted genome reconstruction, sheds further light on metabolic potential of the Methanomassiliicoccales. *PeerJ* 2018;**6**:e5614.

Su G, Zopfi J, Yao H *et al.* Manganese/iron-supported sulfate-dependent anaerobic oxidation of methane by archaea in lake sediments. *Limnol Oceanogr* 2020;**65**:863-875.

Timmers PHA, Welte CU, Koehorst JJ *et al.* Reverse Methanogenesis and Respiration in Methanotrophic Archaea. *Archaea* 2017;**2017**, DOI: 10.1155/2017/1654237.

Valenzuela EI, Padilla-Loma C, Gómez-Hernández N *et al.* Humic Substances Mediate Anaerobic Methane Oxidation Linked to Nitrous Oxide Reduction in Wetland Sediments. *Front Microbiol* 2020;**11**:587.

Weber HS, Habicht KS, Thamdrup B. Anaerobic Methanotrophic Archaea of the ANME-2d Cluster Are Active in a Low-sulfate, Iron-rich Freshwater Sediment. *Front Microbiol* 2017;**8**:619.

Welte CU, Rasigraf O, Vaksmaa A *et al.* Nitrate- and nitrite-dependent anaerobic oxidation of methane. *Environ Microbiol Rep* 2016;**8**:941–55.

Wik M, Varner RK, Anthony KW *et al.* Climate-sensitive northern lakes and ponds are critical components of methane release. *Nat Geosci* 2016;**9**:99–105.

Wood ED, Armstrong FAJ, Richards FA. Determination of nitrate in sea water by cadmium-copper reduction to nitrite. *J Mar Biol Assoc United Kingdom* 1967;**47**:23–31.

Yu L, He D, Zhang E *et al.* Electricity from anaerobic methane oxidation by a single methanogenic archaeon Methanosarcina barkeri. *Chem Eng J* 2021;**405**:126691.

Zheng Y, Wang H, Liu Y *et al.* Methane-Dependent Mineral Reduction by Aerobic Methanotrophs under Hypoxia. *Environ Sci Technol Lett* 2020;**7**:606–12.

Table 1. Station coordinates, depth, temperature and O_2 concentration measured approximately 50 cm above the sediment surface and NO_3^- concentrations measured 5 cm above the sediment. Loss on ignition (LOI) was measured from the top 0.5 cm of the sediment.

Station	N	E	Depth (m)	Temp (°C)	O_2 (µmol L^{-1})	NO_3^- (µmol L^{-1})	LOI (%)
1	61.03.046	25.03.606	14	9.3	254	60.0	14.6
2	61.03.192	25.05.449	22	6.4	314	62.0	13.4
3	61.03.487	25.06.163	52	5.4	303	45.5	14.2

Fig. 1

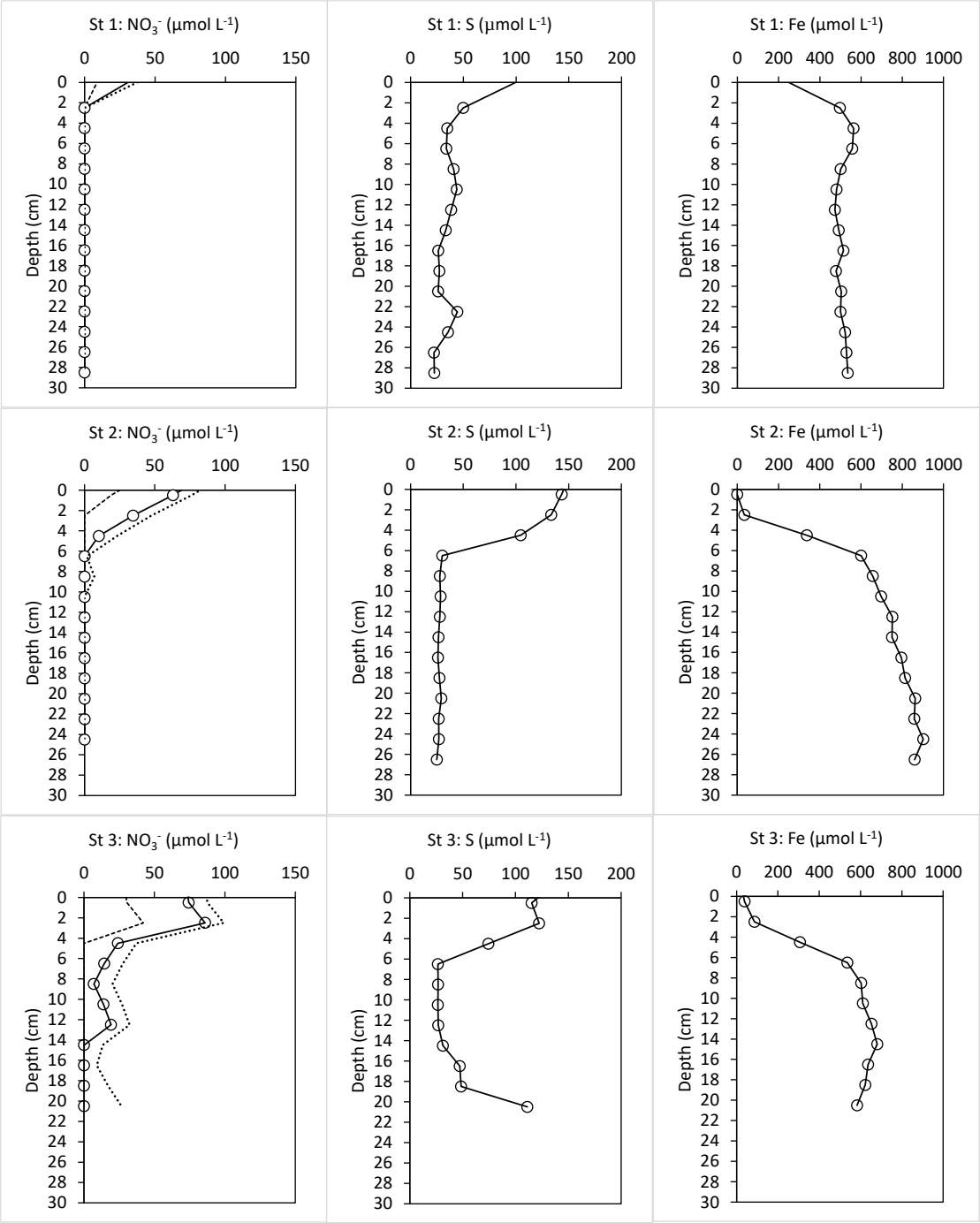

Figure 1. Sediment porewater profiles of dissolved NO_3^- (left panels), S (middle panels) and Fe (right panels) at Stations 1 (upper panels), 2 (middle panels) and 3 (lower panels). Data points from the water overlying the sediment, collected 2.5 cm above the sediment surface, are not shown. The extent of the NO_3^- contamination resulting from HNO_3 washing of porewater samplers was tested and the NO_3^- data is presented as values from which average (solid line with symbols), minimum and maximum contamination (dotted lines) was subtracted (see Materials and Methods). To allow comparison with the microbiological data, the profiles are specifically shown for the top 10 cm layer also in Figure 3.

Fig. 2

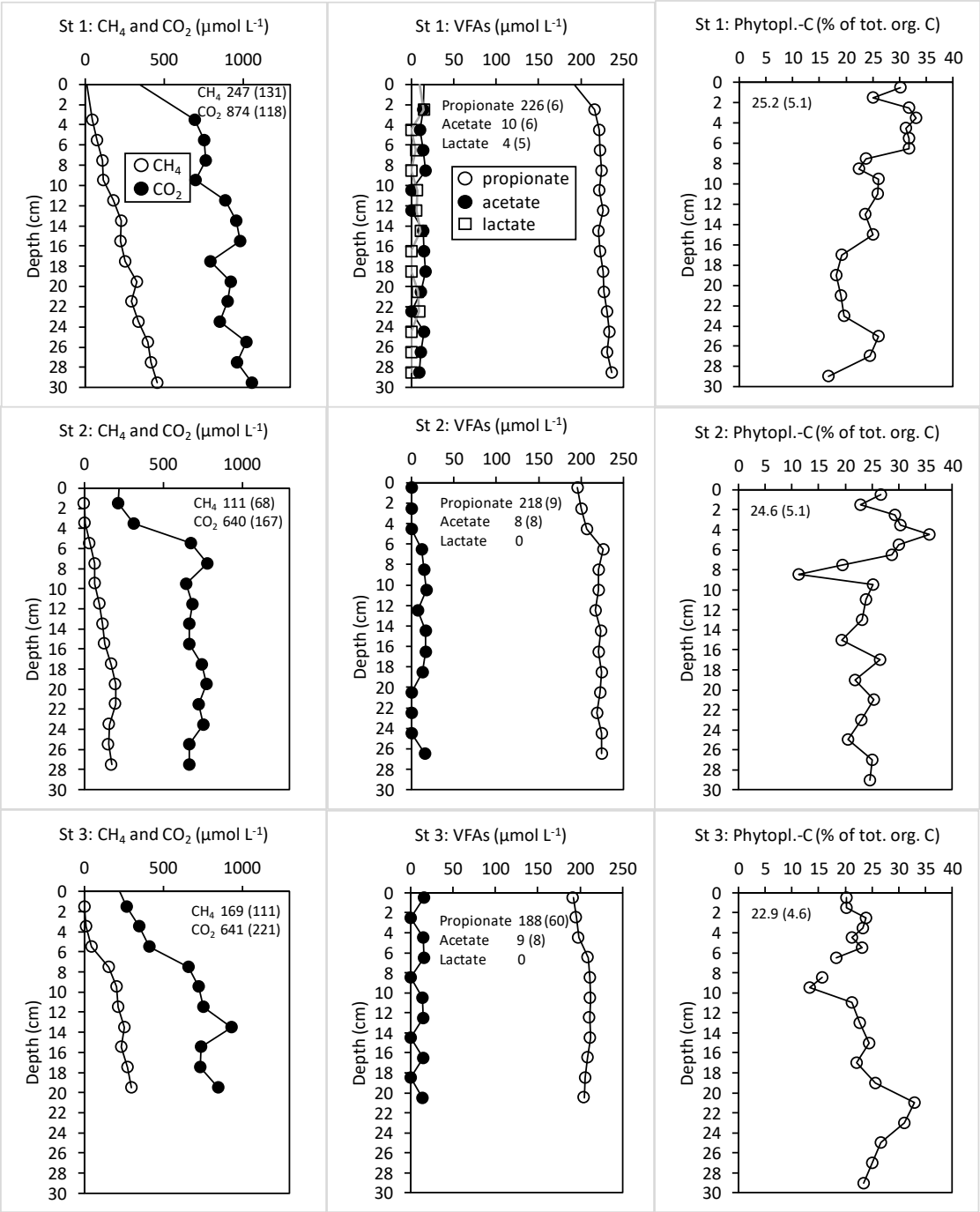

Figure 2. Profiles of CH_4 and CO_2 (left panels), porewater volatile fatty acids (VFAs) (middle panels) and estimated contribution of labile phytoplankton-derived organic carbon in total organic carbon in sediments (right panels) at Stations 1 (upper panels), 2 (middle panels) and 3 (lower panels). Data points from the water overlying the sediment, collected 1 cm and 2.5 cm above the sediment surface for gases and VFAs, respectively, are not shown. The numbers within figures denote average (±SD) calculated across the profiles. To allow comparison with the microbiological data, the profile of CH_4 is specifically shown for the top 10 cm layer also in Figure 3.

Fig. 3

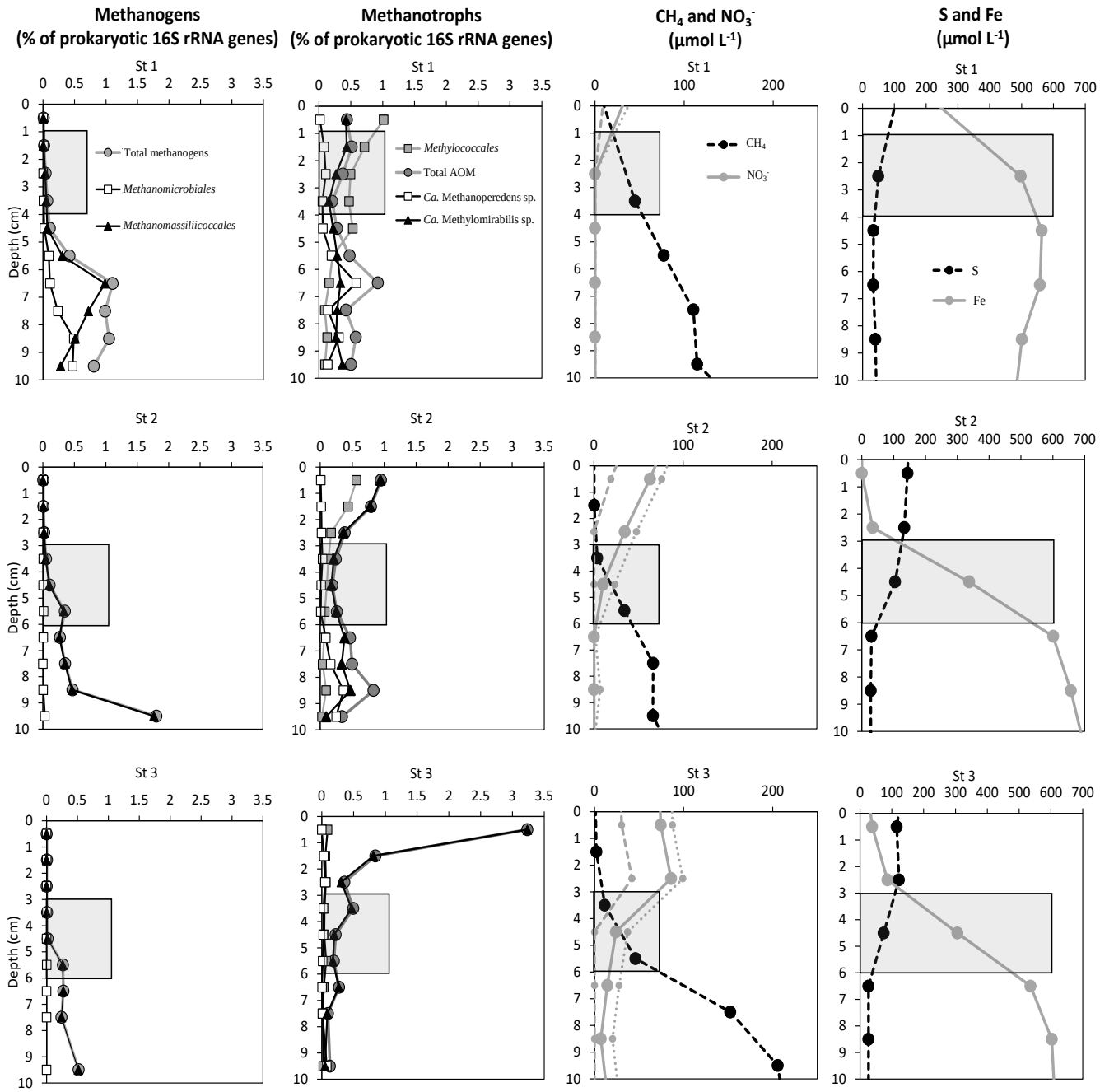

Figure 3. Vertical depth profiles of methanogens (left panels) and methanotrophs (second left panels) based on 16S rRNA gene amplicon sequencing, as well as CH_4, NO_3^- (second right panels), S and Fe (right panels) in the topmost 10 cm of sediments at Stations 1 (upper panels), 2 (middle panels) and 3 (lower panels). The layers chosen for AOM incubation analyses are highlighted with grey color. See Figure 1 for explanation on the presentation of the NO_3^- data.

Fig. 4

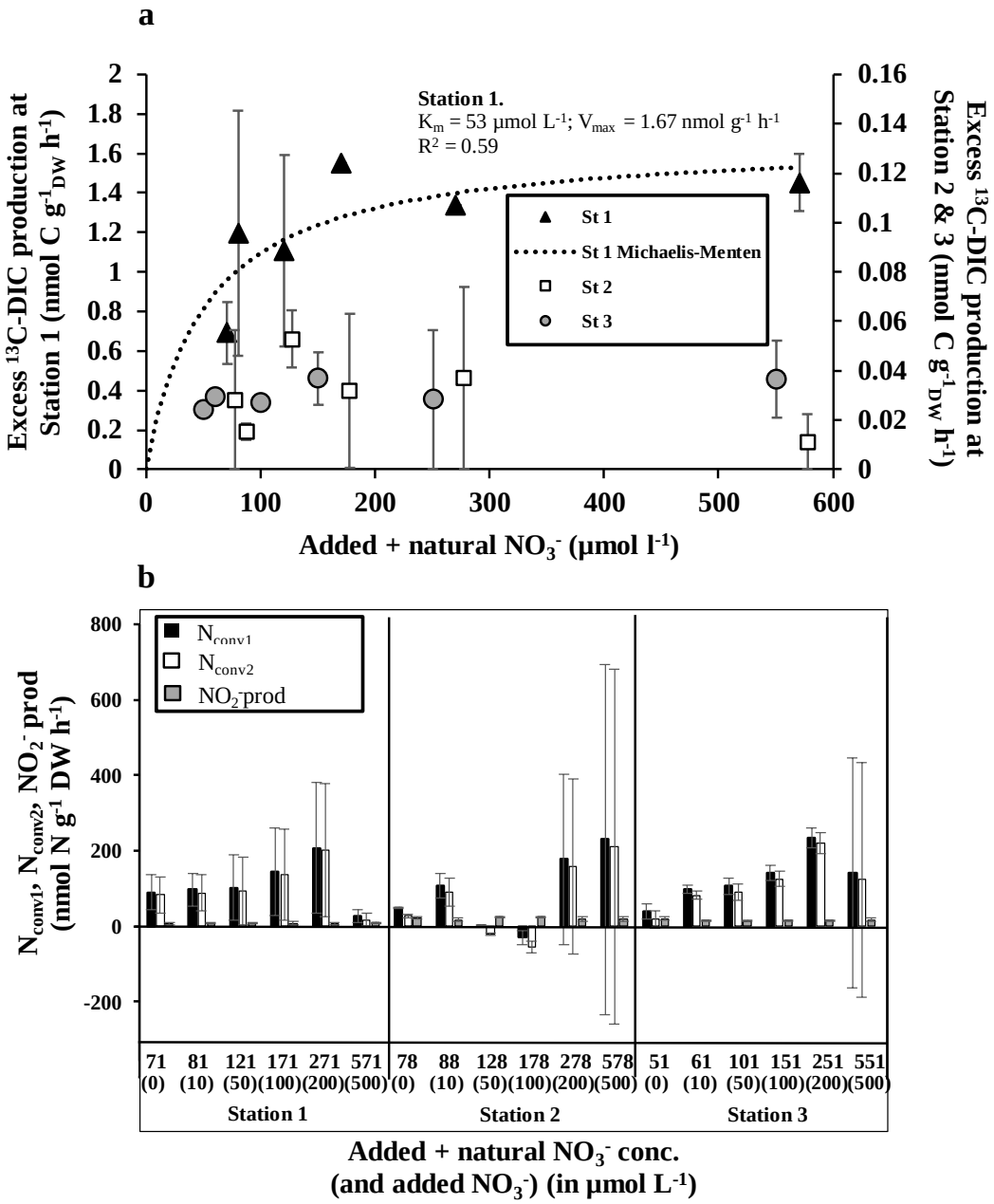

Figure 4. a) Potential AOM rate, i.e. production of excess ^{13}C-DIC, and b) consumption of total NO_3^- to other products (N_{conv1}) and to products other than NO_2^- (N_{conv2}) as well as production of NO_2^- at Station 1 – 3 and at varying NO_3^- concentrations. Values are represented as average +/- average deviation of two replicates, except for AOM at added + natural NO_3^- of 271 µmol L^{-1} at Station 1, where one replicate value was discarded, because it had clearly lower AOM rate (0.25 nmol C g^{-1}_{DW} h^{-1}) than other samples at that station, which was due to problems in either ^{13}C-gas injection or ^{13}C-analysis (in a). Note different y-axes for Station 1 than for other stations (in a). Michaelis-Menten kinetics curve (and K_m and V_{max}) is shown for Station 1. No positive relationship between NO_3^- and AOM was observed for Station 2 and 3 (in a).

Fig. 5

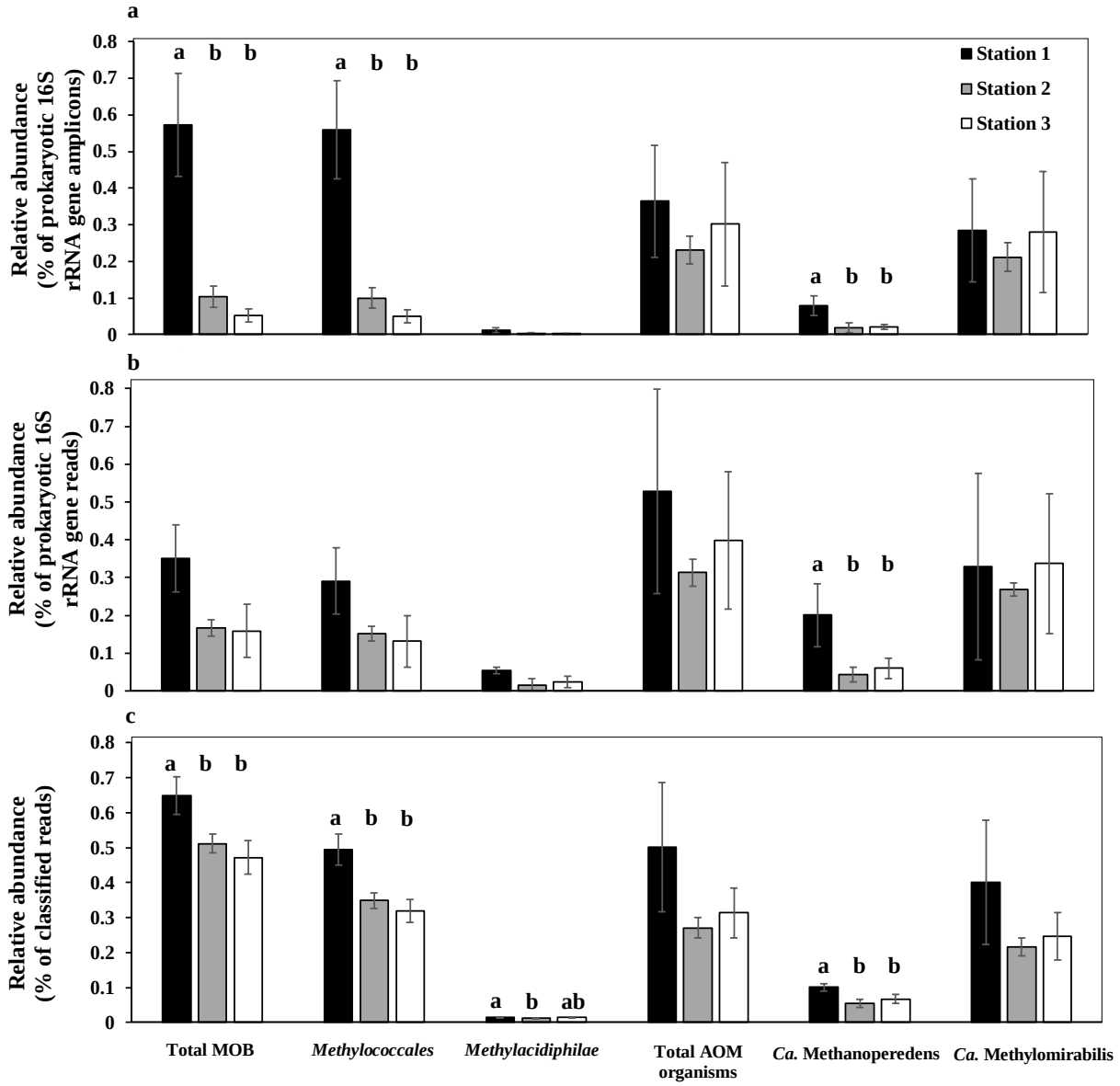

Figure 5. Relative abundance of total aerobic and anaerobic methanotrophs and different methanotrophic taxa in the depth layers representing the incubation layers based on a) 16S rRNA gene amplicon sequencing, as well as b) 16S rRNA gene reads and c) all KAIJU-classified reads in shotgun metagenomic sequence set. Data is represented as an average and standard deviation of three layer-specific samples. Different letters above bars indicate significant differences in RB-ANOVA and subsequent pairwise tests ($p < 0.05$).